RSC Advances

ROYAL SOCIETY OF CHEMISTRY

www.rsc.org/advances

Cite this: DOI: 10.1039/c0xx00000x

www.rsc.org/xxxxxx

ARTICLE TYPE

Feasibility tests of -SO_3H/-SO_3^--functionalized magnesium phyllosilicate [-SO_3H/-SO_3^- MP] for environmental and bioenergy applications

Hyun Gu Kang,[‡a] Kyoung Min Lee,[‡a] Saehae Choi,[b] Bora Nam,[c] Sun-A Choi,[c] Soon-Chang Lee,[d] Ji-Yeon Park,[c] Go-Woon Lee,[e] Hyun Uk Lee,[*f] and Young-Chul Lee[*a]

Received (in XXX, XXX) Xth XXXXXXXXX 20XX, Accepted Xth XXXXXXXXX 20XX

DOI: 10.1039/b000000x

We have prepared a simple water-solubilized, transparent, and anionic clay. –SH-functionalized magnesium phyllosilicate [-SH MP] was easily oxidized into –SO_3H/-SO_3^--functionalized magnesium phyllosilicate [–SO_3H/-SO_3^- MP] by treatment of 5.0% H_2O_2 at 60°C for 24 hours, showing a pH of ~2.0. These water-solubilized and anionic nanoparticles (NPs) were tested with organo-building blocks of –SO_3H/-SO_3^- MP for removal of cationic pollutant dye (methylene blue) and heavy metals (Cd^{2+} and Pb^{2+}). Furthermore, interactions of ubiquitous humic acid (HA) with -SO_3H/-SO_3^- MP were removed due to ion exchange mechanism. For bioenergy applications, glucose conversion from cellulose was tested, focusing on Brønsted acid-rich sites in –SO_3H/-SO_3^- MP.

Introduction

Organic-inorganic building-block behaviors in aqueous solution have emerged for self-assembly of nano-objects or patterns, which induces wrapping or precipitation systems in bionanotechnology[1,2] and environmental engineering.[3,4] Recently, among diverse phyllosilicate clays, the sol-gel-organized phyllosilicate family has emerged as a hot issue due to the high density of primary amine (i.e., aminoclays)[5,6] or thiol organic pendents (i.e., -SH MP)[7,8], mass-produced under ambient conditions by a simple one-pot method.[9] Specifically, water-solubilized and cationic-zeta-potential aminoclays among the phyllosilicate family,[10,11] showing homogeneous nanoparticles (NPs) in aqueous solution,[12] can effectively interact with negatively charged target molecules, ions or other particles, generally within a few minutes.[13,14] As another phyllosilicate clay, -SH MP has provided higher removal capacities for heavy metals,[7,8] but which was not both water-solublized and acted as organo-building blocks. It is indicated that the interaction of certain (nano)materials with oppositely charged anionic organo-building blocks of phyllosilicate clays do not have to be reported yet, due to in the absence of lack of directly utilized and proper organosilane precursors. If developed water-solubilized (water dispersible) and anionic phyllosilicate clays,[12,13,15] likewise the previous aminoclays, are also expected to have useful applications in the (bio)energy, environmental, and medical fields.

Herein it is reported, following two steps for phyllosilicate clay. After preparation of –SH MP, a –SO_3H/-SO_3^--functionalized magnesium phyllosilicate [–SO_3H/-SO_3^- MP) of ~2.0 pH by 5.0%-H_2O_2-based 60°C full 24 hour oxidation of as-prepared -SH MP as a precipitate in aqueous solution, was produced. As a result, –SO_3H/-SO_3^- MP with a homogenous system in aqueous solution was tested for its environmental-application feasibility for removal of cationic methylene blue (MB), heavy metals, and ubiquitous water-soluble humic acid (HA); it was also tested as a polysaccharide hydrolysis catalyst for its bioenergy-application potential with respect to its glucose production from two types of cellulose using abundant Brønsted acid sites.

Materials and methods

Synthesis of -SO_3H/-SO_3^- MP solution

Prior to preparation of -SO_3H/-SO_3^- MP, -SH MP was synthesized following the procedure available in the literature.[1,7,8,16] Briefly, 8.4 g of $MgCl_2$•$6H_2O$ salt (Jusei, Japan) was dissolved into a 200 mL ethanol solution for 10 min stirring. Then, 1.3 mL of (3-mercaptopropyl)trimethoxysilane (MTES) (Sigma-Aldrich, USA) was added, followed immediately by 10 mL of 5.0 M NaOH solution (Daejung, Korea) to induce sol-gel reaction under ambient conditions.[16] After 24 hours reaction, white slurry was produced. After 6,000 x*g* centrifugation for 10 min, ethanol washings were performed 2 times. A 24 hours drying process in a 60°C oven was conducted to evaporate the remaining ethanol to get -SH MP sample. Subsequently, the sample was powdered again by pestle and mortar. Finally, 0.2 g of -SH MP was dispersed in 30 mL teflon-coated polypropylene (PP) bottles containing 18 mL of deionized water, to which 3.5 wt% and 5.0 wt% H_2O_2 concentrations were adjusted.[17] The solution was then hydrothermally treated at 60°C for 24 hours to induce –SH oxidation and ultimately produce -SO_3H/-SO_3^- MP.

Morphological observation of as-prepared –SH and -SO_3H/-SO_3^- MPs by electron microscopy (EM)

1.0 mg/mL of respective -SH MP and -SO_3H/-SO_3^- MP in aqueous solution were dropped onto a carbon-coated copper grid on paper tissue (KIMTECH, Yuhan-Kimberly, Korea) to adsorb water in the sample, which was then examined under 200 kV transmission electron microscopy (TEM, Tecnai F20model, Netherlands).

For only cellulose and -SO_3H/-SO_3^- MP-treated cellulose, the sample was dropped onto tape and examined under cold-type field-emission scanning electron microscopy (FE-SEM, SEM-

4700) at 0.5–30 V and 1 pA–2 nA as well as elemental X-ray analysis (EDX) in the 4 Be – 92 U range.[3]

Characterization of -SO_3H/-SO_3^- MP by spectroscopic methods

For confirmation of the crystalline structure and impurites in –SH powder and -SO_3H/-SO_3^- film MPs, micro-area X-ray diffractometry (D/MAX-2500, RIGAKU) and multi-purpose thin-film X-ray diffractometer (D/MAX-2500, RIGAKU) with normal scan mode at 40 kV and 300 mA were recorded from 3° to 70° in 0.01 step size increments and 3°/min rate, respectively. In order to check the covalent bonding between organic groups in –SH and -SO_3H/-SO_3^- MPs, the Fourier transform infrared (FT-IR) spectra were recorded by spectrometry (FT-IR 4100, Jasco, Japan), preparatory to which the FT-IR sample was prepared with KBr (90 wt%) and –SH or -SO_3H/-SO_3^- MPs (10 wt%). For analysis of elemental-composition and chemical binding species of the -SO_3H/-SO_3^- MP surface, high-resolution X-ray photoelectron spectroscopy (HR-XPS) utilizing monochromatic Al Ka X-ray radiation at a power of 120 W (Kratos Analytical, AXIS Nova, UK) was employed. For -SO_3H/-SO_3^- MP, the shift in the binding energy (eV) due to relative surface charging was corrected and curves were fitted, based on an internal standard (the C1s level at 284.69 eV). For confirmation of condensation degree of Si in -SO_3H/-SO_3^- MP sample, a ^{29}Si cross polarization (CP) magic angle spinning (MAS) 500 MHz liquid nuclear magnetic resonance (NMR) spectrometer (Agilent, VNMRS) was operated at room temperature using tetramethylsilane (TMS) as the reference sample where D_2O solvent was used.

Other characterizations of -SO_3H/-SO_3^- MP

Samples were analyzed for hydrodynamic size and zeta potential in aqueous solution by dynamic light scattering (DLS) methods (Zeta-sizer Nano ZS, Malvern, UK). Elemental analysis (EA) of the sulfur (S) composition (%) and X-ray fluorescence (XRF) analysis of the silicon (Si) composition (%) in the -SH MP powder was performed using an elemental analysis analyzer (EA1108 and NA2000, CE Instruments, USA). Also, the silicon (Si) concentration (mg/L) at 11.11 mg/mL of -SO_3H/-SO_3^- MP solution was measured by inductively coupled plasma atomic emission spectroscopy (ICP-AES, Varian, USA). The sample pH was measured with a pH/ion meter (D-53, Horiba, Kyoto, Japan).

Experimental methylene blue (MB), heavy metals (Cd^{2+} and Pb^{2+}) and humic acid (HA) removals

The cationic dye (methylene blue, MB) was calibrated at 664 nm, resulting in an MB concentration of 0-5.0 mg/L with < 1.0 absorbance intensity. At 2 mg/L of 20 mL MB and according to the -SO_3H/-SO_3^- MP concentrations (1.11, 3.33, 5.55, 8.88, and 11.11 mg/mL), MB-removal experiments were performed by UV-Vis spectrophotometry (Varian, Cary 5000) at the temperature of 18 ± 2°C.

For heavy-metals (respective Cd^{2+} and Pb^{2+})-removal testing, 30 mg/L of both cadmium chloride ($CdCl_2$, Sigma-Aldrich, USA) and lead chloride ($PbCl_2$, Sigma-Aldrich, USA) were mixed in 1.11 mg/mL -SO_3H/-SO_3^- MP kinetically. The heavy metals were analyzed with permeate solution by 0.1 μm syringe filter (Sartorius, Germany) using inductively coupled plasma atomic emission spectroscopy (ICP-AES, Varian, USA). Experiments were performed in duplicate, and the results were averaged.[4]

Likewise, for humic acid (HA)-removal testing, 100 mg/L of HA was mixed with various -SO_3H/-SO_3^- MP concentrations (1.67, 2.22, and 2.78 mg/mL). Then, after having been let stand for 30 min, tests by survery scanning in UV-Vis spectrophotometry (Varian, Cary 5000) were conducted for supernatant solution at the temperature of 18 ± 2°C.

Experimental hydrolysis of cellulose by -SO_3H/-SO_3^- MP

0.2 g of α-cellulose (Sigma-Aldrich, USA) and microcrystalline cellulose (Sigma-Aldrich, USA) in 200 mg of -SO_3H/-SO_3^- MP in an 18 mL water solution (11.11 mg/mL) were prepared in Teflon-coated polypropylene (PP) bottles. According to temperature (100, 120, and 150°C) and hydrothermally auto-claved time (6, 12, and 24 hours), the solutions were tested. After filtering with a 0.1 μm syringe (Sartorius, Germany), high-performance liquid chromatography (HPLC) was performed. The HPLC system (Shimadzu Co., Japan), incorporating a Bio-Rad Aminex HPX-87H analytical column (300 mm × 7.8 mm) and a Cation H microguard cartridge (30 mm × 4.6 mm) (Bio-Rad Laboratories Inc., Hercules, CA) was used for carbohydrate measurement. The column, maintained at 60°C with 5 mmol/L H_2SO_4 eluent (flow rate: 0.6 mL/min), allows for concurrent analysis of acetic and formic acids as well as glucose. The sugar peaks were detected by RI detector (Shimadzu Co., Japan) and identified and quantified by comparison with the retention times of authentic standards.[18] Data were averaged with three runs by repeated experimental samples.

Results and discussion

Preparation of –SO_3H/-SO_3^- MP

In the **Fig. 1a** top panel, schematic pictures of as-prepared –SH MP conversion to –SO_3H/-SO_3^- MP by 3.5% H_2O_2 oxidation via partial delamination of –SH MP to full 5.0% H_2O_2 oxidation of -SO_3H/-SO_3^- MP are depicted, corresponding to digital camera images and transmission electron microscopy (TEM) microphotographs in the bottom panel (**Fig. 1b**). The color of –SH MP in aqueous solution shows opaque but full 5.0% H_2O_2 oxidation of –SH MP to -SO_3H/-SO_3^- MP displayed a transparent and homogenous condition via translucent state of –SO_3H/-SO_3^- MP by 3.5% H_2O_2 oxidation of –SH MP. The morphology of the –SH MP exhibited layer-stacked sheets of a clay structure, which was in good agreement with previous reports on the phyllosilicate family.[5,7,8] However, morphological alternation with a fractal-like tree structure, by partial delamination of electrostatic repulsion between the clay sheets, was observed. At 5.0% H_2O_2 oxidation, the process afforded well-dispersed organo-building blocks of 20-200 nm diameters of -SO_3H/-SO_3^- MP.

Spectroscopic characterizations

–SH and –SO_3H/-SO_3^- MPs spectral characterizations are shown in **Figure 2**. For confirmation of the crystalline structure and indentification of –SH and -SO_3H/-SO_3^- MPs, **Figure 2a** presents that –SH MP displayed the 2:1 trioctahedral smectite structure at 2θ=~60° of the $d_{060,330}$ plane. Notably, the mesolamellar-layered distinct peak on the d_{001} spacing with 1.25 nm at 2θ=7.09° in **inset of Fig. 2a** which was disappeared by oxidation of the –SH groups to –SO_3H/-SO_3^- ones. The mesolamellar peak in –SO_3H/-SO_3^- MP was disappeared due to randomly distribution of organo-building blocks. The disappearance of d-spacing at (001) plane in –SO_3H/-SO_3^- MP was sometimes observed in re-assembling of

organo-building blocks of aminoclay,[19] with typical amorphous phyllosilicate clay structure at 2θ=9.55° at d_{002} and 21.62° at $d_{020,110}$ and a weak intensity of 2θ=35.26° at $d_{130,200}$ in –SO_3H/-SO_3^- MP.[7,8] Moreover, the broad in-plane peaks at d_{002}, $d_{020,110}$, and $d_{130,200}$ in –SH MP matched well with talc-like phyllosilicate, which result is in good agreement with the literature.[5,7,8] In **Fig. 2b**, covalent bonding in –SH MP revealed (ν-OH) at 3,423 cm^{-1}, (ν-CH_2-) at 2,920 and 2,850 cm^{-1}, (δ-OH) at 1,656 cm^{-1}, (νSi-C) at 1,145 cm^{-1}, (νSi-O-Si) at 1,035cm^{-1}, (νC-S) at 693 cm^{-1}, and (νMg-O) at 605 cm^{-1}, as corresponds with the previous data.[8] Although the vibration peak of the –SH-functional group at ~2,550 cm^{-1} was not found in this study,[8] however, most of vibration peaks is matched with those of –SH MP. The vibration peaks in -SO_3H/-SO_3^- MP, those of the –SO_3H/-SO_3^- functional groups were indicated in the 1,340 cm^{-1} – 1,030 cm^{-1} range, in particular 1,196 cm^{-1} of -SO_2 stretching mod and 1,044 cm^{-1} at -SO_3^- stretching mode in -SO_3H groups.[20,21] Focusing on the –SO_3H/-SO_3^- species, XPS survey scans detected O_{1s} at 532.41 eV, C_{1s} at 284.69 eV, S_{2s} at 233.89 eV, and S_{2p} at 170.49 eV (**Fig. 2c**). **Figure 2d** shows 169.87 eV at S_{2p1} and 168.7 at S_{2p3} in -SO_3H and 167.6 eV at S_{2p1} and 166.5 eV at S_{2p3} in -SO_3^-, and further weak curves 167.65 at S_{2p1} and 166.5 eV at S_{2p3} at in-SH with 0.04 and 0.09 of relative area ratios divided by S_{2p3} in -SO_3H.[20,21] This indicated that –SH MP was successfully oxidized to –SO_3H/-SO_3^- MP, leading to anionic charged organo-building blocks in -SO_3H/-SO_3^- MP were delaminated in aqueous solution by repulsion interaction. Additionally, an elemental analysis (EA) revealed the sulfur (S) composition to be ~10.7% (~3.34 mmol/g). Si concentration by XRF technique was

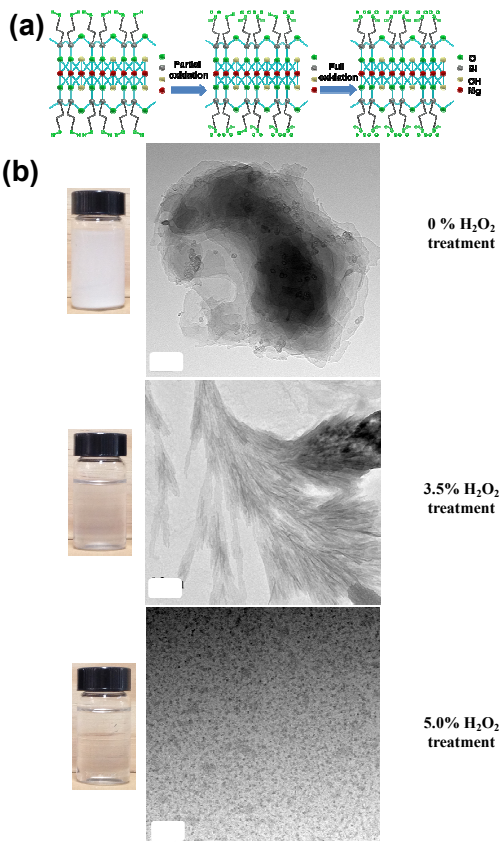

Fig. 1 Schematic representation of -SO_3H/-SO_3^- MP organo-building-block clusters by oxidation of -SH MP. Top panels (a): Approximate unit structure of Mg-phyllosilicate clay according to different concentrations of H_2O_2 oxidation. Bottom panels (b): Corresponding digital camera image of glass vials at 11.11 mg/mL (left) and transmission electron microscopy (TEM) (right) images of respective 0%, 3.5%, and 5.0% H_2O_2 treatment of –SH MP in dispersed water (1.0 mg/mL). All scale bars = 200 nm.

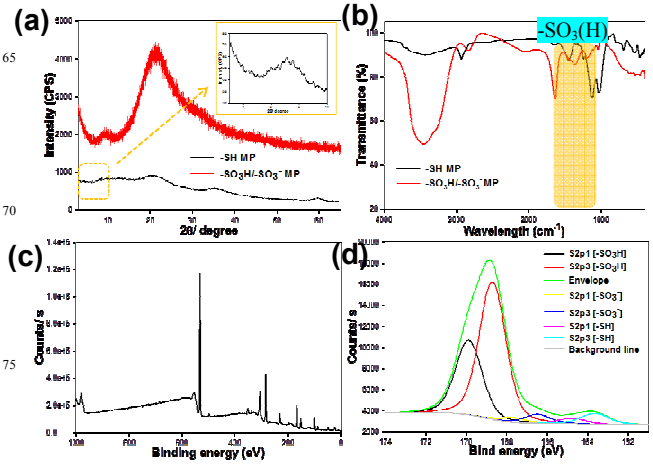

Fig. 2 (a) X-ray diffraction (XRD) pattern spectrum of –SH and -SO_3H/-SO_3^- MPs where inset shows diffraction pattern at low angle of 2θ for –SH MP, (b) pellet-mode Fourier transform infrared (FT-IR) spectrum of –SH and -SO_3H/-SO_3^- MPs, (c) X-ray spectroscopy (XPS) survey scan spectrum of -SO_3H/-SO_3^- MP, and (d) fitting curves of S2p core in -SO_3H/-SO_3^- MP XPS spectrum.

measured to be ~27.4% (~9.78 mmol/g), indicating the Si/S ratio displays ~2.9. The Si concentration of –SO_3H/-SO_3^- MP solution at 11.11 mg/mL was confirmed by ICP-AES measurement, resulting in ~2.054 mg/mL. The degree of Si condensation in –SO_3H/-SO_3^- MP was tested by ^{29}Si-MAS-NMR spectrum of -SO_3H/-SO_3^- MP. It is indicating that showed three signals at −49/−59, −55 to −58/−70, and −67/−78 ppm ppm associated with R-SiO-$(OH)_2$ (T1 signal), R-SiO_2-OH (T2 signal), and R-SiO_3-(T3/Q3 signal) in the inorganic–organic backbone structure of -SO_3H/-SO_3^- MP, displaying mainly a complete condensation of MTES, confirmed by a dominant T3 signal (data not shown).[22]

Environmental application

Using water-solubilized -SO_3H/-SO_3^- MP, methylene blue (MB) as a cationic dye model was tested for removal kinetics in the electrostatic attraction between -SO_3H/-SO_3^- MP and cationic dyes as well as ion exchange process between protons in -SO_3H/-SO_3^- MP, inducing MB removal. **Figure 3a** indicates that 1.11 mg/mL of -SO_3H/-SO_3^- MP showed a transparent property ranging from 200 nm to 700 nm wavelengths with lesser absorbance intensity. The relative absorbance intensity in the UV range is related to the residual H_2O_2 in -SO_3H/-SO_3^- MP solution. As the -SO_3H/-SO_3^- MP concentrations were increased, the absorbance of MB was decreased as a result of adsorption or precipitation by -SO_3H/-SO_3^- MP within a 10 min, due to the electrostatic attraction and ion exchange process between MB molecules and the organo-building blocks of -SO_3H/-SO_3^- MP; this compares with only 2 mg/L of MB at a shoulder peak at ~614 nm and a strong visible peak of 664 nm wavelength, which was

in line with the photographs of discoloration in 2 mg/L of MB (**Fig. 3b**). Further, heavy metals (Cd^{2+} and Pb^{2+}) removal by -SO_3H/-SO_3^- MP at pH ~4.0 was applied kinetically (**Fig. 3c**). Within 5 min, fast removal efficiencies were achieved. For the initial 30 mg/L Cd^{2+} and Pb^{2+} concentrations by 11.11 mg/mL of -SO_3H/-SO_3^- MP, they demonstrated 0.81 and 1.35 mg/g (heavy metal per -SO_3H/-SO_3^- MP) of removal capacities in a homogenous system. The removal rate of heavy metals (Cd^{2+} and Pb^{2+}) by -SO_3H/-SO_3^- MP resulted in 2.959 x 10^{-3} and 7.925 x 10^{-3} min^{-1}, respectively. This fast-removal phenomenon is similar to oxyanion removal by water-soluble aminoclay.[4] Taking into consideration the real practical environment, ubiquitous organic matter can affect in the heavy metal removal behavior of the -SO_3H/-SO_3^- MP colloidal. **Figure 3d** exhibits the interaction of water-soluble humic acid (HA) according to -SO_3H/-SO_3^- MP concentrations. With increased -SO_3H/-SO_3^- MP concentrations, HA removal occurred by ion exchange mechanism and decrease of HA solubility in aqueous solution by decrease in pH as well as electrostatic interaction with microenvironmental sites in macromolecular HA.[23] In the **inset of Fig. 3d**, it can be seen that the brown-colored HA in the supernatant solution became transparent by precipitation. At 100 mg/L HA, 2.78 mg/mL of -SO_3H/-SO_3^- MP showed a ~98% decrease of turbidity within 30 min. Cationic amine groups in macromolecular HA can interact mainly with -SO_3H/-SO_3^- MP or ion exchange driving force. Generally, in the presence of organic matter, heavy-metals removal by -SO_3H/-SO_3^- MP was not inhibited, because HA, simultaneously, also played a role in their removal of heavy metals.[4]

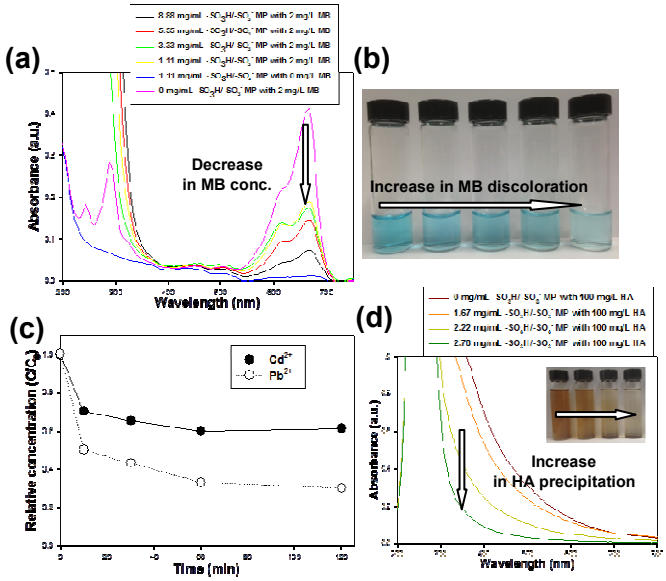

Fig. 3 (a) UV-vis absorbance spectra of 2 mg/L MB concentration according to -SO_3H/-SO_3^- MP loadings, (b) its digital camera photograph, (c) heavy-metal removal kinetics of 11.11 mg/mL -SO_3H/-SO_3^- MP, and (d) UV-vis absorbance spectra of 100 mg/L HA according to -SO_3H/-SO_3^- MP loadings, where the inset shows its digital camera photograph.

Bioenergy application

To test the bioenergy application by water-solubilized and Brønsted acid-rich -SO_3H/-SO_3^- MP, glucose production for α-cellulose and microstalline cellulose by hydrolysis according to hydrothermal temperatures (100, 120, and 150°C) and auto-clave times (6, 12, and 24 hrs) was evaluated. The averged products yields by high-performance liquid chromatography (HPLC) analysis are summarized in **Table 1**. Under the 150°C and 12 hrs conditions, the highest glucose production yields, 0.850 g/L and 1.066 g/L for 10 g/L of respective α-cellulose and microstalline cellulose in aqueous solution, were obtained. The higher glucose yield for microstalline cellulose than that for α-cellulose is attributable to the finer powder (i.e., smaller particle size with higher surface area) affording easier access to polysaccharide hydrolysis contacting sites in the catalystic functionalites. Under the optimal hydrothermal auto-claved treatment of microcrystalline cellulose, formic acid and acetic acid (g/L) were produced, as by-products via glucose intermediates, in 1.213 and 1.039 g/L yields, respectivley, particularly which amounts were nearly equivalent to those of glucose.

Figure 4 shows the surface-morphological alternations of cellulose after hydrolysis with -SO_3H/-SO_3^- MP treatment. Smooth pristine α-cellulose surfaces (**Figs. 4a and b**) were changed to rough surfaces with many holes after hydrolysis by 11.11 mg/mL of -SO_3H/-SO_3^- MP treatment for 11.11 mg/mL of α-cellulose (**Figs. 4c and d**).[24,25] Note that the red-dotted rectangular boxes can be easily discerned in **Figs. 4a-d**.

Table 1 Hydrolysis of cellulose by –SO_3H/-SO_3^- MP

Cellulose type	Temperature (°C)	Time (hour)	Glucose (g/L)	Formic acid (g/L)	Acetic acid (g/L)
α-cellulose	100	6	0.135	-	-
		12	0.142	-	-
		24	0.136	-	-
	120	6	0.210	-	-
		12	0.378	-	-
		24	0.288	-	-
	150	6	0.364	1.230	0.962
		12	0.850	1.579	1.015
		24	0.725	1.803	1.195
Microcrystalline cellulose	100	6	0.310	-	-
		12	0.278	-	-
		24	0.361	-	-
	120	6	0.290	-	-
		12	0.353	-	-
		24	0.465	-	-
	150	6	0.306	0.854	0.899
		12	1.066	1.213	1.039
		24	1.054	1.677	1.167

Note that the - symbol indicates "not measured".

Hydrolysis occurred gradually from the outside to the inside of α-cellulose with accessible Brønsted acid-rich -SO_3H/-SO_3^- MP.[20,26] The surface charge of -SO_3H/-SO_3^- MP was measured to ~-8.65 mV of zeta potential value. For the mixture of α-cellulose and -SO_3H/-SO_3^- MP in aqueous solution, the zeta potential was ~-0.0654 mV. After α-cellulose hydrolysis treatment at 150°C and 12 hours with -SO_3H/-SO_3^- MP, the hydrodynamic size of the α-cellulose with -SO_3H/-SO_3^- shrunk from ~25.14 μm to ~14.69 μm. **Figure 4e** shows the -SO_3H/-SO_3^- MP coated on the hydrolyzed α-cellulose surface. The presence of C and O in elemental-composition analysis (**Fig. 4f**) is sourced from both α-cellulose and -SO_3H/-SO_3^- MP, while the Mg, Si, S, and Cl compositions indicates the presence of -SO_3H/-SO_3^- MP, because in the absence of -SO_3H/-SO_3^- MP, compositions of Mg, Si, S,

and Cl were not detected in only α-cellulose. Thus, it is believed that -SO_3H/-SO_3^- MP is potential catalyst for hydrolysis of polysaccharides as a heterogeneous catalyst. However, immobilization of mechanically and thermally stabilized -SO_3H/-SO_3^- MP onto macro-sized matrixes is suggested as a practical commercial means of facile catalyst recovery.

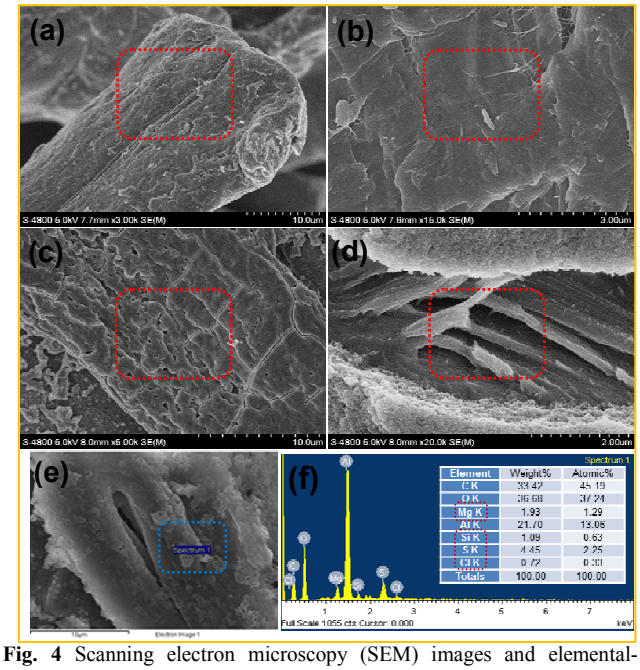

Fig. 4 Scanning electron microscopy (SEM) images and elemental-composition analysis after -SO_3H/-SO_3^- MP treatment with α-cellulose: (a,b) original α-cellulose; (c,d) α-cellulose by -SO_3H/-SO_3^- MP treatment; (e) α-cellulose by -SO_3H/-SO_3^- MP treatment and (f) its energy-dispersive X-ray (EDX) analysis for selected area of (e). In (f), note that the dotted red box indicates the presence of -SO_3H/-SO_3^- MP in the dotted blue box in (e).

Conclusions

In summary, we developed a water-solubilized and anionic magnesium phyllosilicate [-SO_3H/-SO_3^- MP] with pH ~2.0. The homogeneity of this clay in aqueous solution enabled fast removal of cationic dye, heavy metals, and HA as a novel adsorbent for environmental engineering applications. Additionally, Brønsted acid-rich -SO_3H/-SO_3^- MP showed potential as a hydrolysis catalyst for glucose conversion from cellulose by hydrothermal autoclaved treatment, yielding approximately ~10% glucose production at 150°C and 12 hrs. We are currently pursuing the means of utilization of this water-solubilized and anionic clay in the following applications: as an electrolyte in washing agents for electrokinetic (EK) remediation of heavy-metal-contaminated soils; as a Nafion® membrane composite for direct methanol fuel cells (DMFC), and as a self-assembled biomass-conversion catalyst with dual acidity/basicity by mixing two water-solubilized clays containing -SO_3H/-SO_3^- and –NH_2/-NH_3^+ organo-functional groups, i.e., combination of two-dimensional materials with unique properties.

Acknowledgements

This subject is supported by Korea Ministry of Environment as "The GAIA project" and by Gachon University's Cube Research Program of Creative Korea (CK); it as also supported by the New & Renewable Energy Technology Development Program of the Korea Institute of Energy Technology Evaluation and Planning (KETEP) funded by the Korean Ministry of Knowledge Economy (No. 20123010090010).

Notes and references

[a]*Department of BioNano Technology, Gachon University, 1342 Seongnamdaero, Sujeong-gu, Seongnam-si, Gyeonggi-do 461-701, Republic of Korea.*
E-mail: dreamdbs@gachon.ac.kr. (Prof. Y.-C. Lee)
[b]*Environmental Biotechnology Research Center, Korea Research Institute of Bioscience & Biotechnology (KRIBB), Daejeon 305-806, Republic of Korea*
[c]*Biomass and Waste Energy Laboratory, Korea Institute of Energy Research (KIER), 152 Gajeong-ro, Yuseong-gu, Daejeon 305-343, Republic of Korea*
[d]*Department of Fine Chemical Engineering and Applied Chemistry, Chungnam National University, Daejeon 305-764, Republic of Korea*
[e]*Testing and Certification Center, Korea Institute of Energy Research (KIER), 152 Gajeong-ro, Yuseong-gu, Daejeon 305-343, Republic of Korea*
[f]*Advanced Nano-Surface Research Group, Korea Basic Science Institute (KBSI), Daejeon 305-333, Republic of Korea*
E-mail: leeho@kbsi.re.kr. (Dr. H.U. Lee)
‡ *These authors contributed equally to this work.*

1 S. Mann, *Nat. Mater.*, 2009, **8**, 781-792.
2 A. J. Patil and S. Mann, *J. Mater. Chem.*, 2008, **18**, 4605-4615.
3 Y.-C. Lee, S.-J. Jang, M.-H. Choi, T.-J. Jeon, T. Ryu, Y. S. Huh, *Appl. Catal. B-Environ.*, 2013, **142-143**, 494-503.
4 Y.-C. Lee, W.-K. Park and J.-W. Yang, *J. Hazard. Mater.*, 2011, **190**, 652-658.
5 S. Mann, S. L. Burkett, S. A. Davis, C. E. Fowler, N. H. Mendelson, S. D. Sims, D. Walsh and N. T. Whilton, *Chem. Mater.*, 1997, **9**, 2300-2310.
6 K. K. R. Datta, A. Achari and M. Eswaramoorthy, *J. Mater. Chem. A*, 2013, **1**, 6707-6718.
7 M. G. Fonseca and C. Airoldi, *Thermochim. Acta*, 2000, **359**, 1-9.
8 I. Lagadic, M. K. Mitchell and B. D. Payne, *Environ. Sci. Technol.*, 2001, **35**, 984-990.
9 Y.-C. Lee, E. S. Jin, S. W. Jung, Y.-M. Kim, K. S. Chang, J.-W. Yang, S.-W. Kim, Y.-O. Kim and H.-J. Shin, *Sci. Rep.*, 2013, **3**, 1292(1-8).
10 P. Chaturbedy, D. Jagadeesan and M. Eswaramoorthy, *ACS Nano*, 2010, **4**, 5921-5929.
11 K. K. R. Datta, C. Kulkarni and M. Eswaramoorthy, *Chem. Commun.*, 2010, **46**, 616-618.
12 K. K. R. Datta, M. Eswaramoorthy and C. N. R. Rao, *J. Mater. Chem.*, 2007, **17**, 613-615.
13 Y.-C. Lee, E. J. Kim, D. A. Ko and J.-W. Yang, *J. Hazard. Mater.*, 2011, **196**, 101-108.
14 Y. Hwang, Y.-C. Lee, P. D. Mines, Y. S. Huh and H. R. Andersen, *Appl. Catal. B-Environ.*, 2014, **147**, 748-755.
15 A. Achari, K. K. R. Datta, M. De, V. P. Dravid and M. Eswaramoorthy, *Nanoscale*, 2013, **5**, 5316-5320.
16 S. L. Burkett, A. Press and S. Mann, *Chem. Mater.*, 1997, **9**, 1071-1073.
17 C. H. Rhee, H. K. Kim, H. C. Chang and J. S. Lee, *Chem. Mater.*, 2005, **17**, 1691-1697.
18 J.-Y. Park, M. Kang, J. S. Kim, J.-P. Lee, W.-I. Choi and J.-S. Lee, *Bioresour. Technol.*, 2012, **123**, 707-712.
19 A. J. Patil, E. Muthusamy and S. Mann, *J. Mater. Chem.*, 2005, **15**, 3838-3843.

20 K. Nakajima and M. Hara, *ACS Catal.*, 2012, **2**, 1296-1304.
21 R. Jia, J. Ren, X. Liu, G. Lu and Y. Wang, *J. Mater. Chem. A*, 2014, **2**, 11195-11201.
22 Y.-C. Lee, Y.-S. Choi, M. Choi, H. Yang, K. Liu and H.-J. Shin, *App. Clay Sci.*, 2013, **83-84**, 474-485.
23 M. Cerff, M. Morweiser, R. Dillschneider, A. Michel, K. Menzel and C. Posten, *Bioresour. Technol.*, 2012, **118**, 289-295.
24 X. Li, Y. Jiang, L. Shuai, L. Wang, L. Meng and X. Mu, *J. Mater. Chem.*, 2012, **22**, 1283-1289.
25 S. Suganuma, K. Nakajima, M. Kitano, D. Yamaguchi, H. Kato, S. Hayashi and M. Hara, *J. Am. Chem. Soc.*, 2008, **130**, 12787-12893.
26 J. A. Melero, L. F. Bautista, G. Morales, J. Iglesias and R. Sánchez-Vázquez, *Chem. Eng. J.*, 2010, **161**, 323-331.

TOC

We developed a water-solubilized and anionic magnesium phyllosilicate [-SO_3H/-SO_3^- MP] with pH ~2.0, enabling applications in both environmental engineering and bioenergy.